Progress in Organic Coatings 174 (2023) 107296

Contents lists available at ScienceDirect

Progress in Organic Coatings

journal homepage: www.elsevier.com/locate/porgcoat

Corrosion resistance enhancement of a sol-gel coating by incorporation of modified carbon nanotubes: Artificial neural network (ANN) modeling and experimental explorations

Sajjad Akbarzadeh [a,b], Kazem Akbarzadeh [c], Mohammad Ramezanzadeh [d], Reza Naderi [a,*], Mohammad Mahdavian [d], Marie-Georges Olivier [b,*]

[a] School of Metallurgy and Materials Engineering, College of Engineering, University of Tehran, Tehran, Iran
[b] Department of Materials Science, Faculty of Engineering, University of Mons, 20 Place du Parc, 7000 Mons, Belgium
[c] Abadan Faculty of Petroleum Engineering, Petroleum University of Technology, Abadan, Iran
[d] Department of Surface Coatings and Corrosion, Institute for Color Science and Technology, P.O. Box 16765-654, Tehran, Iran

ARTICLE INFO

Keywords:
Silane
Corrosion
Artificial neural network (ANN)
EIS
Multi-walled carbon nanotube (MWCNT)

ABSTRACT

A computational method of data analysis based on an artificial neural network (ANN) has been proposed to model the behavior of a sol-gel coating modified with different amounts of oxidized multi-walled carbon nanotubes (O-MWCNT). The constructed ANN model utilized a single hidden-layer perceptron. The Levenberg–Marquardt algorithm optimization procedure was applied as a learning algorithm. In this model, the input variables were the different concentrations of O-MWCNT, the immersion time, and the real part of the impedance, and consequently, the imaginary part of the impedance was considered as the output variable. Then, the accuracy of the optimized model was evaluated using the correlation coefficient and schematically comparing the simulated data with the experimental ones in the Nyquist diagrams. Furthermore, the protection performance of the sol-gel layer was enhanced by the incorporation of O-MWCNTs. To this end, the different concentrations of the O-MWCNTs up to 0.9 % wt./wt. have been added to a silane layer, and the performance was followed by electrochemical exploration using electrochemical impedance spectroscopy (EIS). The results revealed the improvement of the protective performance of the silane coating by increasing the content of the O-MWCNTs in the matrix, followed by the enhancement of barrier properties. Moreover, the polarization curves, in agreement with the AC impedance spectra, reflected the significant decrease in the corrosion current density by employing more content of O-MWCNTs in the silane-based coatings.

1. Introduction

Over the past 25 years, the EIS technique has been utilized for the electrochemical characterization of protective coatings applied on metallic substrates. The most widely used method to interpret the spectra determined by this technique is based on the modeling by an electrical equivalent circuit (EEC). The spectra can be fitted using EEC to obtain electrochemical elements corresponding to the degradation process and protective function of coatings. However, the EIS technique has some limitations including the lack of a suitable electrical equivalent circuit model for some coatings, data scattering, stationarity and linearity, and so signal drift that sometimes happens in low frequencies [1–9]. Therefore, it is necessary to use other techniques and methods along with the EIS technique to keep track of the electrochemical behavior of the coated samples immersed in an aggressive solution.

An Artificial Neural Network (ANN) machine learning model is mathematical modeling that enables solving complex nonlinear mathematical problems in prediction and optimization without any predefined mathematical relationship between its variables. In fact, a neural network is a series of algorithms endeavors to recognize underlying relationships in a set of data through a process that mimics the way used by the human brain to operate. Neural networks refer to systems of neurons, either organic or artificial in nature. They can be adapted by changing the input data; therefore, the network generates the best possible result to redesign the output criteria. The concept of neural networks having their roots in artificial intelligence is swiftly gaining

* Corresponding authors.
E-mail addresses: rezanaderi@ut.ac.ir (R. Naderi), Marjorie.OLIVIER@umons.ac.be (M.-G. Olivier).

https://doi.org/10.1016/j.porgcoat.2022.107296
Received 14 August 2022; Received in revised form 17 October 2022; Accepted 26 October 2022
Available online 9 November 2022

popularity in the development of engineering systems and optimization. Self-learning capability can be considered one of the most important features of ANN. ANN can obtain the empirical relationship between independent and dependent variables [10–12]. Therefore, this mathematical model seems ideally appropriate for the prediction and modeling of EIS data that are known to be complex and nonlinear.

Colorado-Garrido et al. presented a predictive model based on ANN for the electrochemical impedance Nyquist plots at different exposure times to analyze the corrosion resistance of the pipeline steel. In this model, the Levenberg–Marquardt was considered as a training method and the real impedance and time were used as the input variables, and the imaginary part of impedance was obtained as the output variable [13]. A. Bassam et al. proposed an ANN model to determine the type of corrosion in the pipeline steel. In their model, four input variables including the real part of impedance, the imaginary part of impedance, exposure time, and inhibitor concentration were set as input variables [14]. In another study, the real part of the impedance and different chemical compositions of nanocomposite polymer electrolyte system as input and imaginary part of impedance as output were set for the creation of an ANN machine learning model in order to investigate the effect of the chemical composition on the impedance spectra of nanocomposite polymer electrolyte system [15]. Méndez-Figueroa et al. predicted the electrochemical impedance in two SiO_2-nanostructured patinated quaternary bronzes by using statistical tools and feed-forward backpropagation ANN modeling. By using the statistical tools, they found the correlation between the input and output parameters, revealing that some parameters (frequency, corrosion rate, immersion time, real and imaginary part of impedance) had the highest variability [16]. Wang et al. investigated the stray current corrosion process in a chloride solution by employing the combination of electrochemical and ANN analyses [17]. Their ANN model was built up of Nyquist outcome, in which ion concentration, stray current density, corrosion time, and real impedance were the input variables and imaginary impedance was set as the output of the predicted model. In another study, M. Ghobadi et al. achieved accurate results in the prediction of corrosion resistance of a lanolin coating incorporated with inhibitors via ANN [18].

Although many studies have been carried out on ANN to interpret and predict EIS data, some of them have been along with plenty of limitations. The most crucial limitations include the use of trial-and-error methods to optimize the neurons of the hidden layer as well as the lack of immediate access to a large amount of EIS data due to the time-consuming nature of the corrosion tests. Therefore, the purpose of the present study is to develop a new ANN prediction model that simulates the corrosion behavior of the coating after eliminating the mentioned limitations. Consequently, in the first step, the effect of different concentrations of O-MWCNTs including 0.05, 0.3, 0.6, and 0.9 % w/w on the protective performance of a silane layer was investigated. The silane layer was composed of methyltriethoxysilane (MTES), glycidoxypropyltrimethoxysilane (γ-GPS), and tetraethylorthosilicate (TEOS) precursors. Then, an ANN prediction model of different impedance Nyquist plots was developed and trained with experimental data to predict the performance of the coatings. To improve the performance of the traditional neural network in predicting the performance of coatings 101 different criteria were used to optimize the neurons of the hidden layer. Over-fitting is one of the most common problems that occur during ANN training [19]. One strategy that can be used to solve this problem is known as K-fold cross-validation (CV). In this process, the data set is randomly split into a "K" independent subsets or folds wherein each iteration of each subset is used as a testing set while the remaining "K-1" subset is used to train the ANN. Therefore, in each fold, a model is created and, in each model, the network is tested with a new data set [20]. Normally, it is recommended to split the data set into 10 subsets to evaluate the generalization capacity of the network [21]. Consequently, to avoid over-fitting in this paper, a 10-fold CV was used. All calculations were carried out by the Neural Network Toolbox function in MATLAB software version 9.8.0.635 (R2020a).

2. Experimental

2.1. Materials

Silane precursors were tetraethylorthosilicate (TEOS), methyltriethoxysilane (MTES), and Glycidoxypropyltrimethoxysilane (γ-GPS) purchased from Merck Co. (Germany). The silane solution contained ethyl alcohol and acetic acid supplied from Zakaria Jahrom Co. (Iran). Substrate was steel panel with the chemical composition of Fe:97.7, Si:0.415, Mn:1.39, Co:0.0559, C:0.19, Cu:0.0429, Nb:0.0481, Mo: 0.018, and Cr:0.026 wt% acquired from Foolad Mobarakeh Co, Iran. To increase the wettability of the silane layer on the steel panels, an acid pretreatment was performed by using sulfuric acid and benzothiazole (Merck Co.) as pH controller and corrosion inhibitor, respectively. MWCNTs having a wall number of 3–15 were provided by Nanostartech Co. (Iran).

2.2. Oxidation of MWCNTs

0.5 g of MWCNT was poured into a beaker consisting of 0.1 L of sulfuric acid of 75 % and nitric acid of 65 % with a volumetric ratio of 3:1, respectively. Then, the mixture was stirred for a day at 100 °C before adding 0.5 L of distilled water and stirring for 30 min. Next, the solution was centrifuged for 15 min at the rotational speed of 4500 rpm. Finally, the suspension was washed a couple of times with distilled water to create O-MWCNT [22].

2.3. Sample preparation

Mechanical polishing of the steel panels was done with sandpapers starting from 400 to 1000 grit size. Then, the samples were degreased with acetone to prepare a clean surface. Prior to applying the silane coating, specimens were treated with an acidic solution to produce an activated layer on the mild steel surface, leading to the wettability of the coating on the substrate. For this purpose, panels were dipped into a sulfuric solution at pH 3 for 10 s in which benzothiazole was used as an inhibitor followed by rinsing and drying instantly [23,24].

Sol-gel solution with the concentration of 20 % w/w was prepared by magnetically stirring TEOS, MTES, and γ-GPS organosilanes equally for one day in the medium of deionized water and ethyl alcohol in which the pH was set at 3 by means of acetic acid [25].

The influence of oxidation time of carbon nanotubes on the corrosion resistance properties of the silane coating has been studied at one distinct concentration [26]. In this study, different silane nanocomposites coatings (0.05, 0.3, 0.6, and 0.9 % w/w versus the precursor content) were generated by dispersing the various amounts of O-MWCNT into the acidic water with the same pH of the silane solution via ultrasonication with the power of 150 W for half an hour (TOPSONICS instrument). Then, this mixture was added to the silane solution 15 min before the coating fabrication.

The dip-coating method was employed to apply the silane film with/without O-MWCNTs on the acid-treated specimens. Panels were immersed into the neat silane and 0.05, 0.3, 0.6, and 0.9 % silane-based nanocomposite solutions for 1 min with the withdrawal rate of 200 mm/min to produce coated samples denoted as Sil, Sil-C1, Sil-C2, Sil-C3, and Sil-C4, respectively. Finally, the samples were dried at room temperature for 24 h and subsequently placed in an oven at 150 °C for 30 min. The schematic representation of the experimental steps from the oxidation step to the prepared coated sample is depicted in Fig. 1.

2.4. Characterization

Carbon nanotubes were characterized by thermogravimetric analysis (TGA) in the N_2 atmosphere from 25 to 800 °C with a scan rate of 10 °C/min employing STA 1500 instrument. Also, zeta potential (ZP) of the nanotubes immersed at different pHs in the water medium was carried

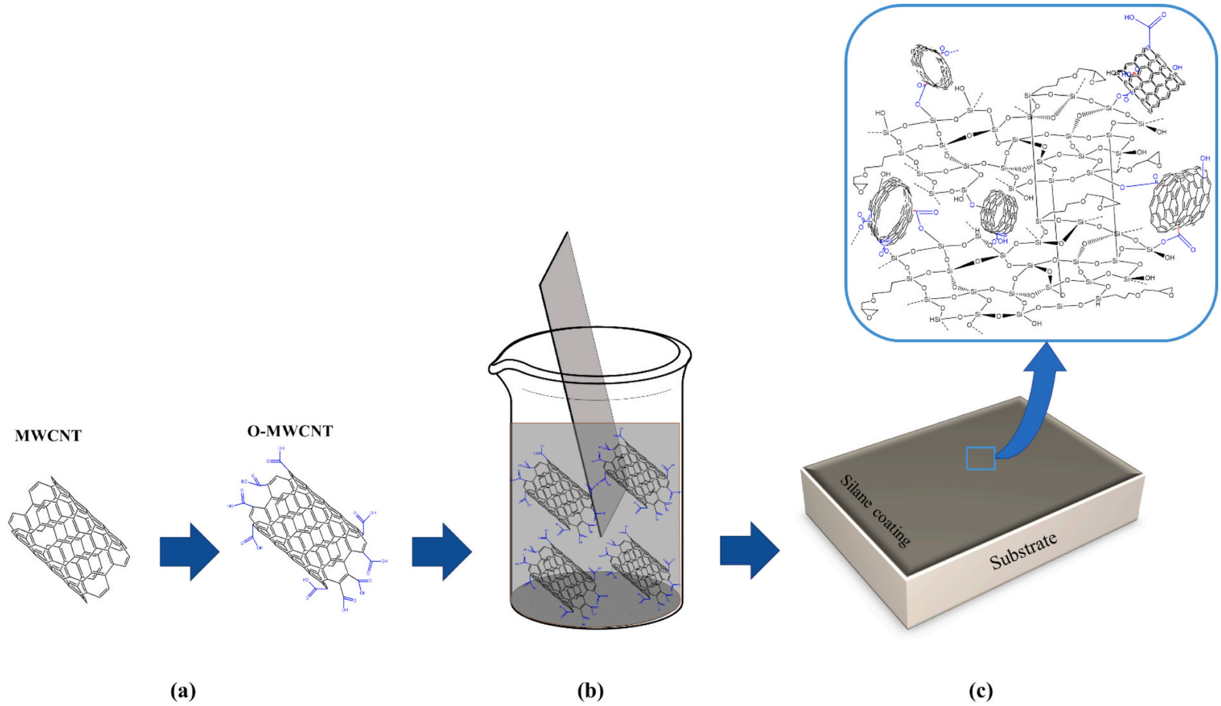

Fig. 1. Schematic illustration of the oxidizing step (a), dip-coating of mild steel panels in silane solution along with O-MWCNTs nanomaterials (b), and the fabricated silane-based nanocomposite coating (c).

out through the Horiba SZ-100 apparatus. The morphology of the O-MWCNT, as well as the silane coating thicknesses, were visualized by field emission scanning electron microscopy (FE-SEM). X-ray diffraction (XRD) test was employed to indicate d-spacing and the phase composition of both pristine and oxidized MWCNT. The PANalytical instrument with the radiation source of Cu Kα in the 2θ domain of 5–80° was exploited. Fourier-transform infrared spectroscopy (FT-IR) analysis was conducted in the wavenumber domain of 4000–450 cm^{-1} utilizing a Perkin-Elmer instrument to examine the effect of different concentrations of O-MWCNTs on the structural properties of the silane network. The hydrophobicity properties of silane coatings with/without various concentrations of O-MWCNTs were studied by water contact angle (WCA) measurement.

2.5. Electrochemical assessment

A three-electrode cell was utilized to investigate the corrosion protection performance of the coated samples with the EIS in 0.1 M NaCl solution. A saturated calomel electrode (SCE), a platinum electrode, and the coated panels were designed as reference, auxiliary, and working electrodes, respectively. The electrochemical response of the samples covered by a mixture of beeswax-colophony except 1 cm^2 was recorded by the Ivium Compactstat instrument at open circuit potential (OCP). EIS tests were done by a sine wave with a peak-to-peak amplitude of 10 mV in the frequency range from 0.01 to 10^4 Hz. Then, the results were fitted by Zview3.1c software to access the electrochemical parameters. For each set of measurements, at least two identical samples were examined to ensure the reproducibility of the EIS outcome. The standard deviation of each reported parameter originated from the fitting of the identical samples in a similar immersion time. Then by elemental comparison between the outcome of each group of samples, the standard deviation was mathematically calculated and reported below the fitting table. To this end, potentiodynamic polarization test was conducted in the potential range of ±250 mV from OCP after 24 h immersion in 0.1 M NaCl solution, utilizing a 1 mV/s scan rate.

For the ANN modeling, the number of input data used in the network was 378 based on the total data points of EIS tests. In fact, the EIS test of each group of samples at a specific immersion time contained around 32 points obtained by the Ivium Compactstat instrument. These data were fed into the neural network in the form of a matrix. Accordingly, each row of the 378 × 3 dimensional matrix represented a specific point of the real part of impedance that was obtained at a certain concentration of O-MWCNT in the silane coating and immersion time. Similarly, each row of the 378 × 1-dimensional matrix represented a specific point of the imaginary part of impedance in the Nyquist diagram.

3. Results and discussion

3.1. Nanotube characterization

3.1.1. ZP and FE-SEM analyses

The effect of the oxidation process on the surface charge of carbon nanotubes was studied by the ZP technique in the pH domain of 3–9 as well as the FE-SEM observation of the tube-like structure of O-MWCNT depicted in Fig. 2. It was comprehended that the O-MWCNT had a lower charge than the pristine MWCNT in the whole interval. In fact, carboxylic acid groups imposed a negative charge on the surface bringing about an electrostatic repulsive force between the nanoparticles. Therefore, the more the repulsive force, the more dispersion stability could be expected in the solgel solution [27]. It is worthwhile to mention that the pristine MWCNT had no charge at the pH of almost 7 which is in parallel with the works of other scientists [28–30].

3.1.2. TGA and XRD results

TGA measurement was performed to analyze the thermal stability of MWCNT before and after the oxidation process. The results are shown in Fig. 3. Only one step of weight loss (about 14 %) can be distinguished at 500 °C in the spectra of MWCNT which was the initiation point of MWCNT decomposition. This result indicated that the pristine MWCNT is not previously functionalized. While MWCNTs might have been contaminated with other impurities during their production explaining the slight decrease of plateau detected before reaching 500 °C. [31,32].

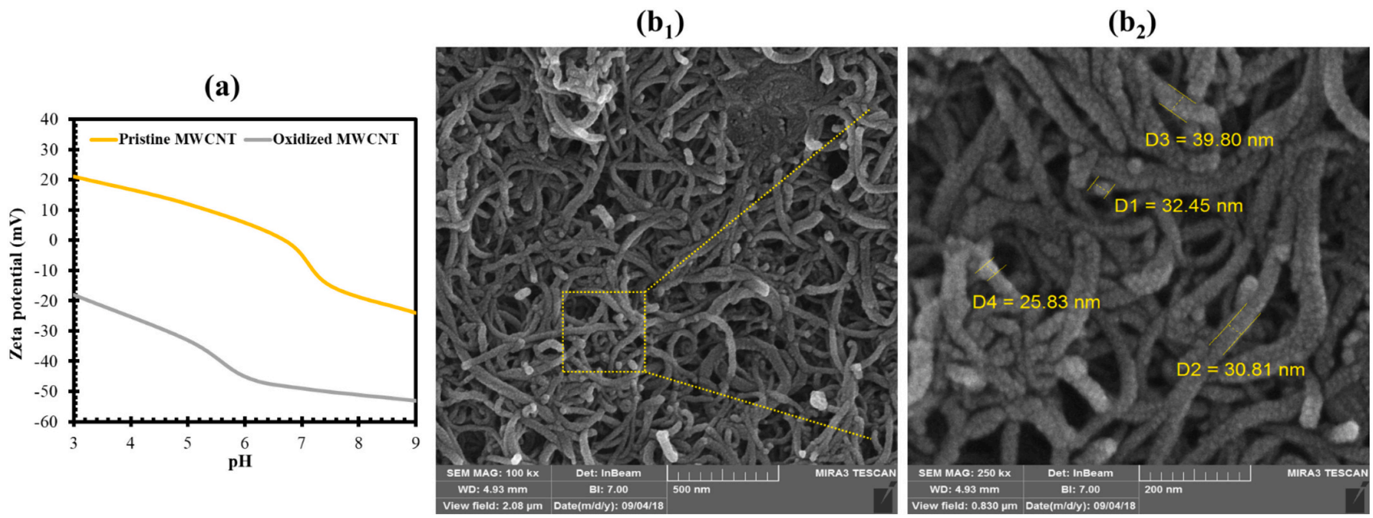

Fig. 2. ZP measurement (a) and FE-SEM observation of O-MWCNT in 100 kX (b_1) and 250 kX (b_2) magnifications.

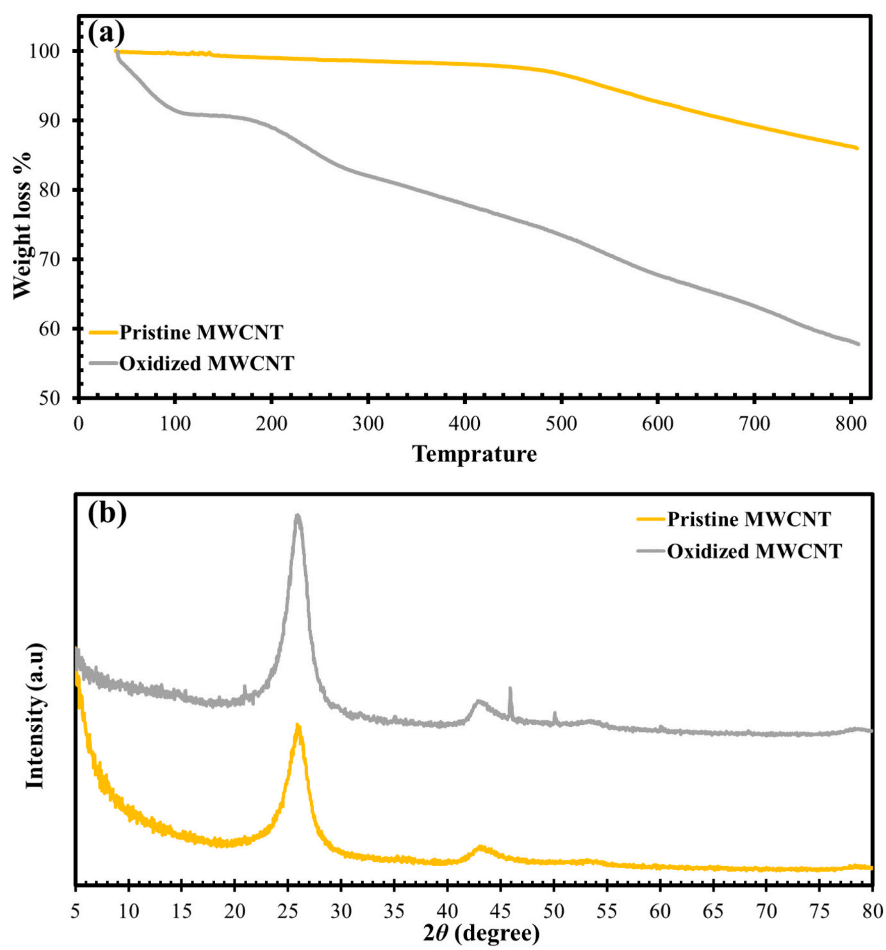

Fig. 3. TGA (a) and XRD (b) outcomes of MWCNT and O-MWCNT.

After the oxidation process, two other steps of weight loss can be seen for O-MWCNT. The first one was attributed to the water evaporation that happens before 100 °C, and the other one which occurs between 100 and 300 °C was related to carboxylic acid decay [33,34]. Based on the graphs, the weight losses for the former and the latter steps were 9 % and 9.5 %, respectively. The successful oxidation of MWCNT and production of the carboxylic acid groups are confirmed.

The XRD patterns of pristine MWCNT and O-MWCNT were also determined in Fig. 3. The two intense peaks at $2\theta = 43^\circ$, 26° were assigned to (1 0 0) and (0 0 2) Bragg reflection planes corresponding to the interlayer spacing and in-plane regularity, respectively [35]. In particular, the diffraction peak at 26° was sharper compared to the rest, illustrating the removal of impurities and amorphous carbon upon the oxidation process of MWCNT. Noteworthy to mention that the d-spacing of the (0 0 2) plane almost remained unchanged after oxidation which was 3.45 Å and 3.42 Å for O-MWCNT and MWCNT, respectively. Moreover, the graphitization degree has not been varied after functionalization which is in agreement with other studies [36,37].

3.2. Coating examination

3.2.1. FT-IR analysis

The effect of different concentrations of O-MWCNT on the structure and network properties of the silane coating was studied by the FT-IR test exhibited in Fig. 4. The stretching and bending vibration modes of O-H can be respectively related to the peaks at 3434 and 1630 cm^{-1} wavenumbers [38]. The C-H vibration peaks at 2876 and 2934 cm^{-1} could likely originate from the γ-GPS and MTES molecules, respectively [39,40]. The presence of intense peaks in the wavenumber domain of 900 to 1200 cm^{-1} revealed the successful silica network formation through hydrolysis and condensation reactions [41]. Specifically, the peaks at 1040 and 1100 cm^{-1} wavenumbers are closely corresponded to the ladder-like and cage-like structures of Si-O-Si, illustrating the formation of more cage-like structures of siloxane after the addition of O-MWCNT to the silane formulation [42,43]. Noteworthy to mention that the interaction between the carboxylic group of O-MWCNT and silanol groups could be evidenced by the Si-O-C shoulder at 1193 cm^{-1} wavenumber. The intensity ratio of Si-O-Si/O-H was evaluated to determine the effect of various concentrations of O-MWCNTs on the silica cluster formation. To enumerate, this ratio was found to be 2.22, 3.55, 5.16, 6.18, and 9.02 for Sil, Sil-C1, Sil-C2, Sil-C3, and Sil-C4, respectively. It may mean that by increasing the content of O-MWCNT in the silane network not only the barrier performance of silane-coated samples was intensified, but also the matrix formation particularly the cage-like structure upon hydrolysis and condensation reactions was promoted.

3.2.2. WCA examination

The WCA measurement data of the silane-coated samples is provided in Fig. 5. The hydrophobicity of the silane coating was enhanced as the concentration of the O-MWCNTs increased. This result was in parallel with the FT-IR outcome, reflecting the number of polar groups such as hydroxyl groups and/or unreacted silanol groups diminished by the incorporation of O-MWCNTs into the coating formulation. Specifically, the Sil-C4 had the highest WCA among samples, revealing the lowest intention of aggressive electrolyte to penetrate through the coating.

3.2.3. FE-SEM observation

The cross-section images of the nanocomposite coating are demonstrated in Fig. 6. At first glimpse, it was comprehended that the thickness of silane coatings was heightened by the addition of O-MWCNT. In particular, the thickness of the Sil, Sil-C1, Sil-C2, Sil-C3, and Sil-C4 samples equals 1.59 ± 0.21, 3.38 ± 0.32, 5.15 ± 0.29, 5.75 ± 0.38, and 6.24 ± 0.35 μm, respectively. The thickness increment probably stems from the viscosity enhancement of silane coating by employing more content of O-MWCNTs [26,44]. Therefore, the higher the content of O-MWCNT, the thicker the silane coating. Vividly, the barrier properties of a coating are intensified as its thickness is enlarged. Therefore, the higher thickness of silane coatings along with the evolution of a more cage-like structure of siloxane could make silane nanocomposites to acts better than the neat silane coating in terms of corrosion resistance properties.

3.2.4. Electrochemical performance of the silane-based nanocomposites

The EIS spectra of the silane-coated samples with different amounts of O-MWCNT after 24 h immersion in 0.1 M NaCl are indicated in Figs. 7 and 8 as Nyquist and Bode graphs, respectively. As can be seen in Fig. 7, whatever the amount of incorporated O-MWCNT, the corrosion protection performance of the neat silane has been enhanced in all cases. The diameter of the Nyquist semi-circles got enlarged by adding O-MWCNT nanoparticles to the matrix illustrating the increment of the barrier performance of the system. The systems showed a two-frequency response which means the corrosion reaction was controlled by both charge transfer and ionic resistance. The semi-circle in high and low frequencies denoted the film resistance (R_f) and charge transfer resistance (R_{ct}), respectively. Considering the term (R_T) which denotes the total resistance of the system as the sum of R_f and R_{ct}, it can be vividly comprehended that Sil-C4 had the maximum anti-corrosion property among the others up to 24 h of immersion in the aggressive medium. The EIS spectra were fitted with an appropriate electrical equivalent circuit (EEC) (Fig. 9) summarized in Table 1. Additionally, the electrolyte and aggressive ions penetrate the coating through the defects and pathways eventually. According to the fact that all kinds of non-ideal surfaces have some roughness and heterogeneity, employing a constant phase element (CPE) instead of an ideal capacitance is a promising way to elucidate EIS results [45,46]. The impedance of the CPE equals:

$$Z_{CPE} = \frac{1}{Y_0 (i\omega)^n} \tag{1}$$

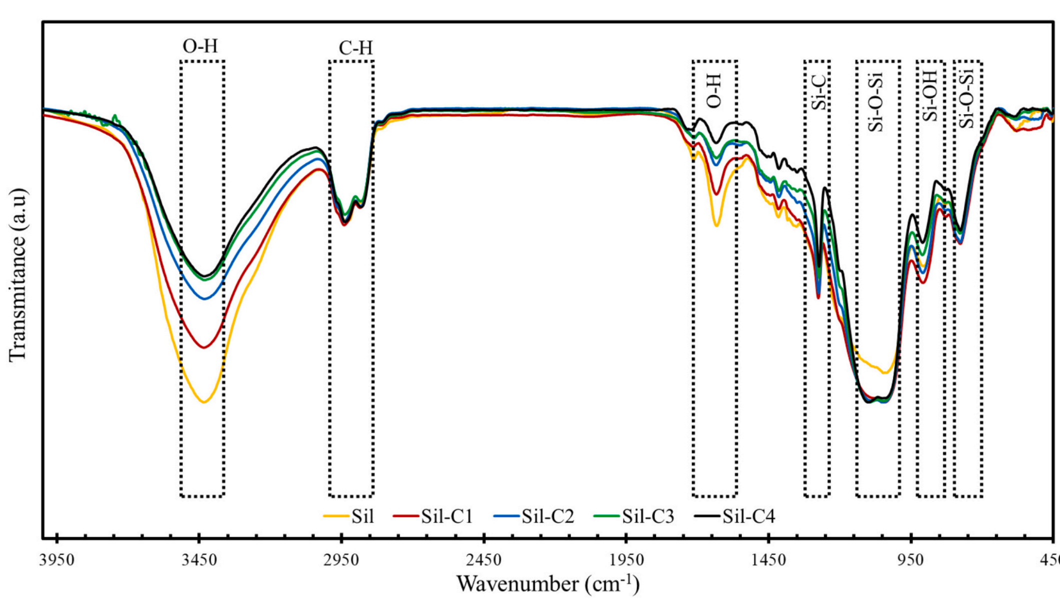

Fig. 4. FT-IR diagrams of silane coatings without/with different contents of O-MWCNT.

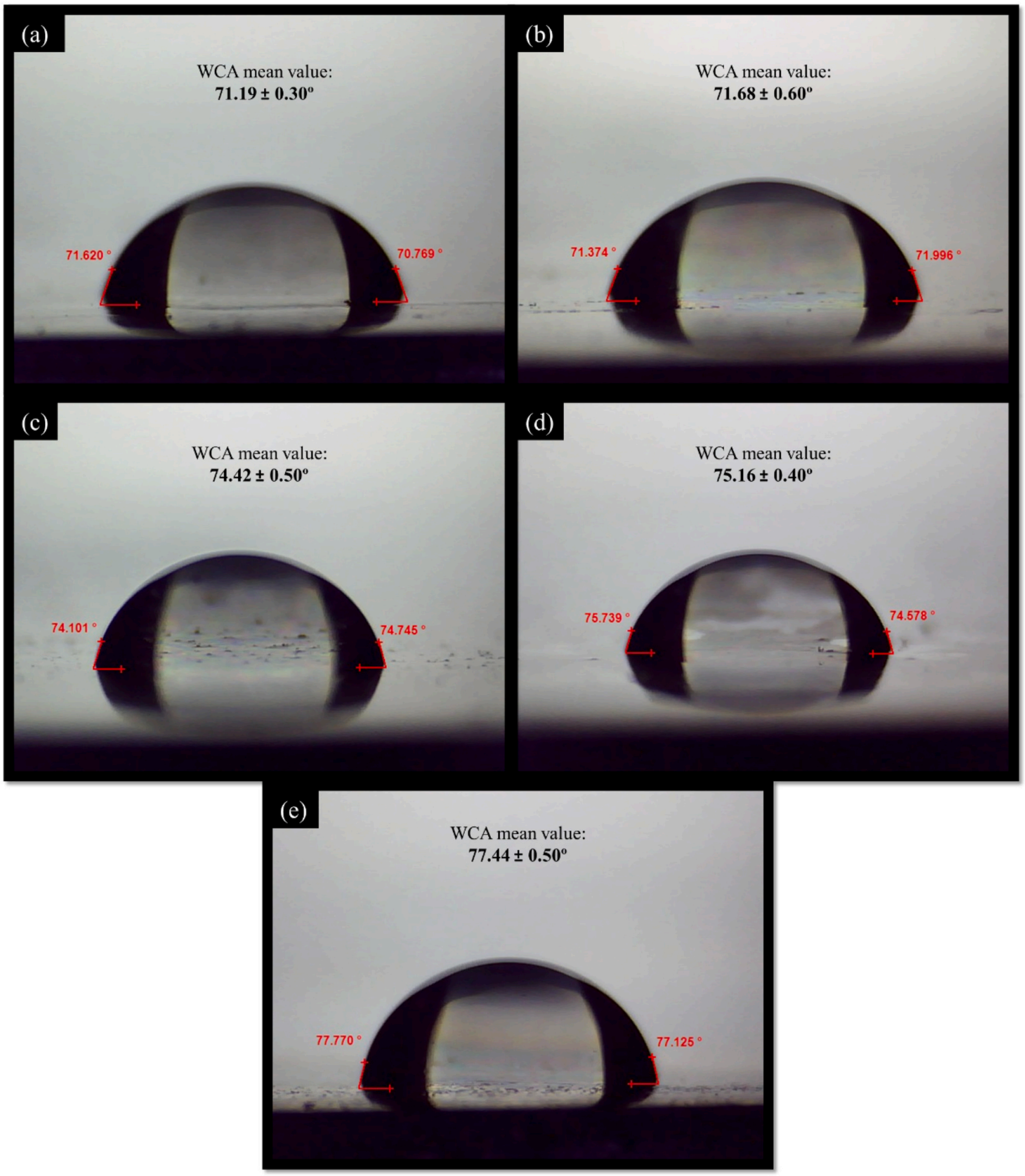

Fig. 5. The WCA evaluation of the coated samples relating to Sil (a), Sil-C1 (b), Sil-C2 (c), Sil-C3 (d), and Sil-C4 (e).

where the admittance of CPE is $Y_{0,}$ and n is the frequency dispersion factor varying from 0 (pure resistance) to 1 (pure capacitance). Apart from the thickening of silane coatings by intake of more O-MWCNT nanoparticles, the ideality of the coating was also enhanced as the n_f exponent of CPE reported in Table 1. In other words, the Sil-C4 sample had not only the highest thickness but also the surface homogeneity and ideality as compared to the Sil sample. By looking at the low-frequency impedance, it was concluded that by elapsing the immersion time the barrier performance of the samples became lower and lower. In contrast, no big difference in the low-frequency impedance between each EIS survey in the Sil-C4 sample is detected with spectra remaining almost stable with immersion time. The EIS result was in good agreement with the FT-IR outcome, illustrating that the increment in the content of O-MWCNT in the silane coating not only increases the barrier performance but also facilitates the siloxane formation upon hydrolysis and condensation reactions. The improvement of barrier properties originated from filling the probable pores and defects in the coating as well as enlarging the diffusion pathways. It should be mentioned that the highest thickness along with its relatively hydrophobic properties of Sil-C4 makes it the best anti-corrosion coating system among others.

3.2.5. Analysis of nanocomposite coating based on ANN model

The considered ANN model was a single hidden-layer perceptron, and the Levenberg-Marquardt (LM) algorithm optimization procedure was applied as a learning algorithm. It has been found empirically that a single hidden layer in the construction of the ANN with an optimum number of nodes would be enough to model many engineering problems [10]. In this work, the activation functions used in the output and hidden layers were linear (Purelin) and hyperbolic tangent sigmoid (Tansig), respectively [47]. The three input layer nodes respectively related to three variables which were the concentration, the exposure time (in hours), and the real part of the impedance, while the output layer node belonged to the imaginary part of impedance (schematically depicted in Fig. 10).

The EIS data set was normalized by linear min-max normalization code before applying it to the network. By using this procedure, all the input and output variables are placed between −1 and 1. The advantages of this method would be listed as speeding up the convergence process,

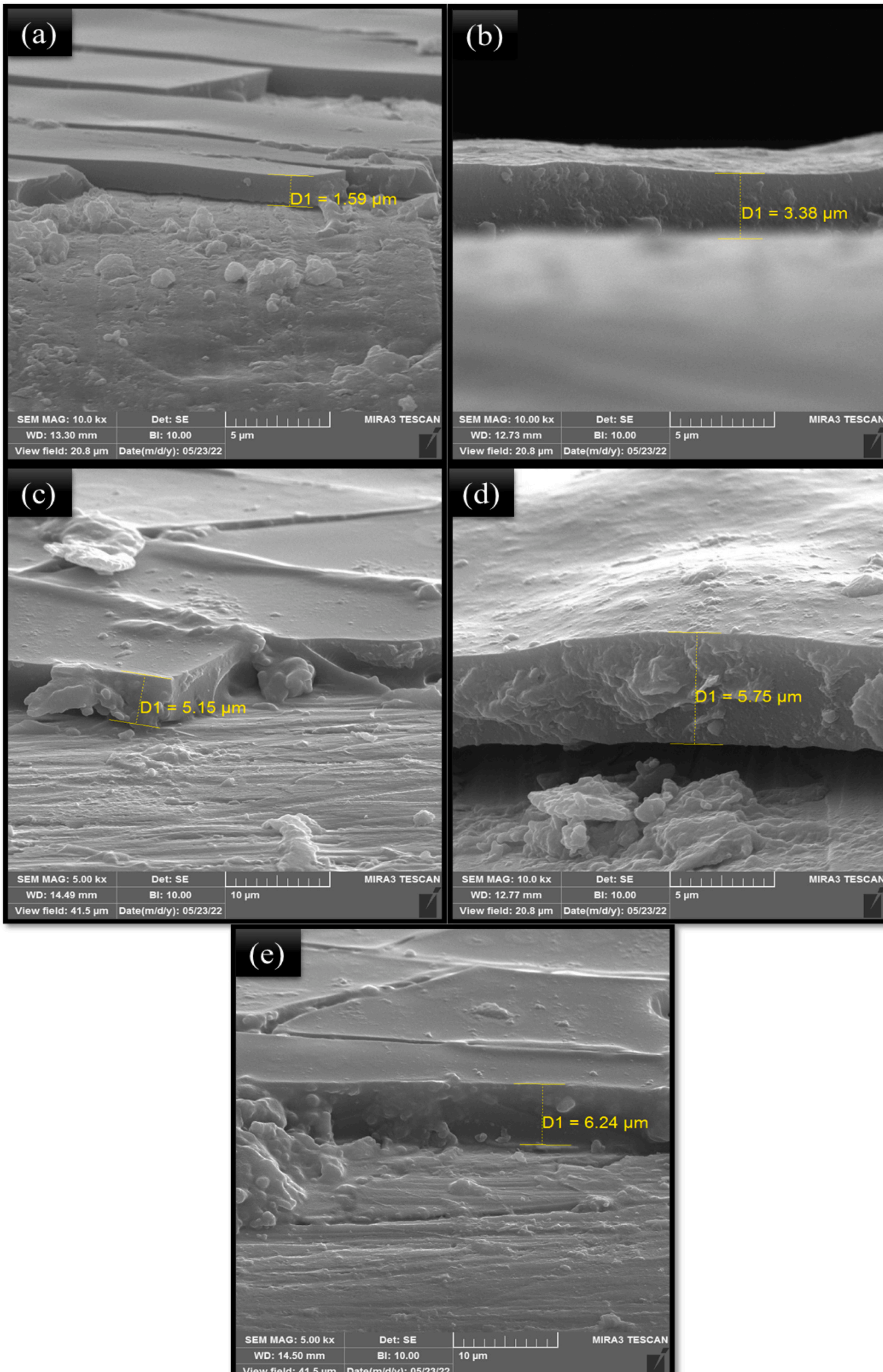

Fig. 6. Cross-section images of different silane coatings corresponding to Sil (a), Sil-C1 (b), Sil-C2 (c), Sil-C3 (d), and Sil-C4 (e).

eliminating the dimensional impact between input indicators, and facilitating ANN learning [48–50]. Data set normalization was obtained by the following transformation:

$$y = \frac{(y_{\max} - y_{\min}) \times (x - x_{\min})}{(x_{\max} - x_{\min})} + y_{\min} \tag{2}$$

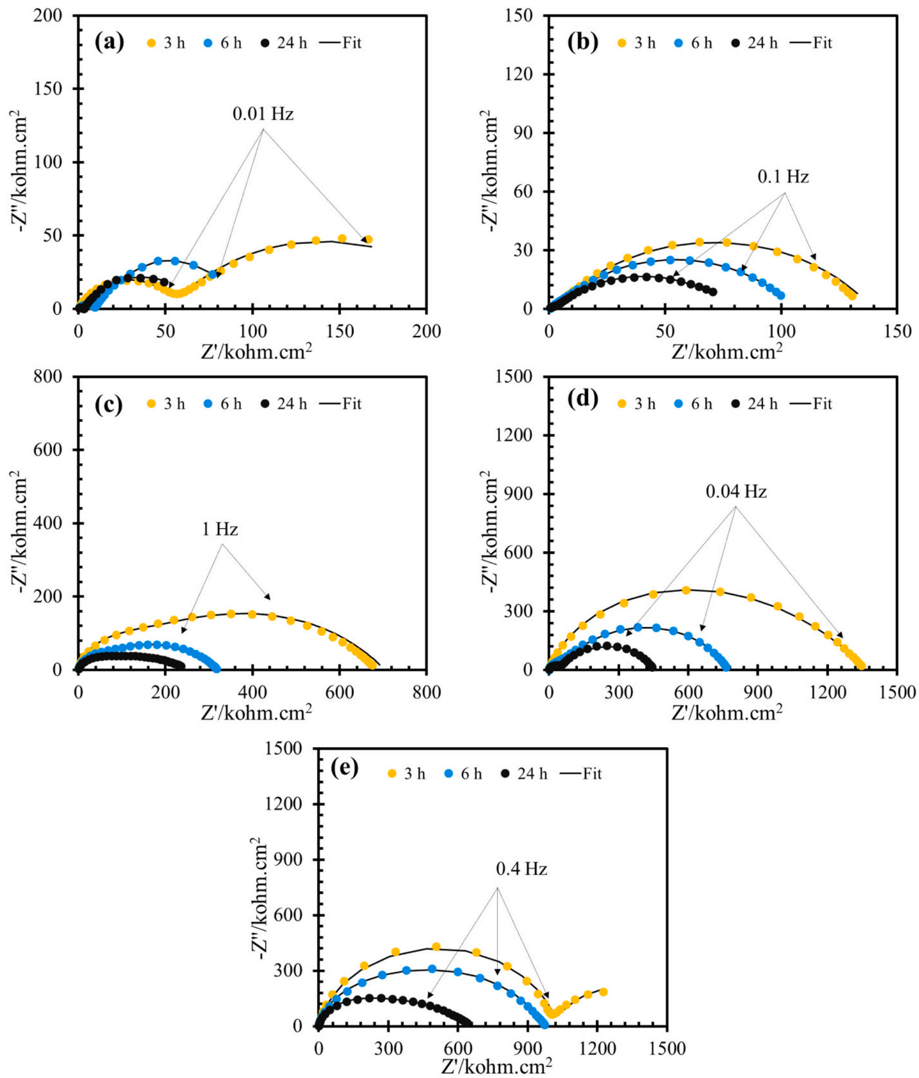

Fig. 7. Nyquist diagrams correspond to the experimental EIS data (marker) plus EEC fitting (solid line) after 24 h immersion in 0.1 M NaCl solution related to Sil (a), Sil-C1 (b), Sil-C2 (c), Sil-C3 (d), and Sil-C4 (e).

where x and y correspond to input and output data, respectively.

The optimal number of hidden nodes in each hidden layer which depends on the complication and type of the fields of study plays an important role in ANN design. If the number of hidden nodes in each hidden layer is more than required then the learning process leads to overfitting of the data; while, a few numbers of hidden nodes are selected, then the model could not find any relations between the input and the target values [51]. At present, the following strategy has been exploited to determine the optimal number of nodes. At first, a series of models of ANN with various numbers of nodes were designed followed by testing each model separately and calculating its learning error. At last, the number of nodes in the model having the lowest error was selected as an optimal number of nodes in a hidden layer of an ANN. In this study, 101 different criteria were evaluated to optimize the number of hidden nodes, and the results were compared with various statistical errors given in Table S1. It is based on the work of Sheela and Deepa who proposed a method to find the number of hidden neurons in a multilayer neural network for wind speed prediction. They reviewed methods to fix several hidden neurons in neural networks for the past 20 years. Then they proposed a new method (101 various criteria) to fix the hidden neurons. This criterion is derived from 101 equations as a function of input neurons (n) that have been substantiated using the convergence theorem. Then they compared this method with other existing models by using statistical errors illustrating that the proposed model could improve accuracy and minimize error [50]. The lowest error is the main basis for the determination of the presented criteria.

The performance of the presented model was evaluated by various statistical error criteria such as Mean Square Error (MSE), Mean Relative Error (MRE), and Mean Absolute Error (MAE) [50].

$$\mathrm{MSE} = \sum_{i=1}^{N} \frac{\left(Y_i'' - Y_i\right)^2}{N} \tag{3}$$

$$\mathrm{MRE} = \frac{1}{N} \sum_{i=1}^{N} \left| \frac{\left(Y_i'' - Y_i\right)}{Y_i} \right| \tag{4}$$

$$\mathrm{MAE} = \frac{1}{N} \sum_{i=1}^{N} \left(Y_i'' - Y_i\right) \tag{5}$$

where Y_i'' and Y_i are the experimental data and predicted data, respectively and N is the total amount of data.

According to Table S1, the best ANN model was the one with the 25 nodes in the hidden layer and its criterion was calculated by using the equation of $(8n + 1) / (n - 2)$. The performance of this model has been evaluated by 3 statistical errors including MSE, MRE, and MAE which were 0.00099606, 0.0020, and 0.0106, respectively. Therefore, it could

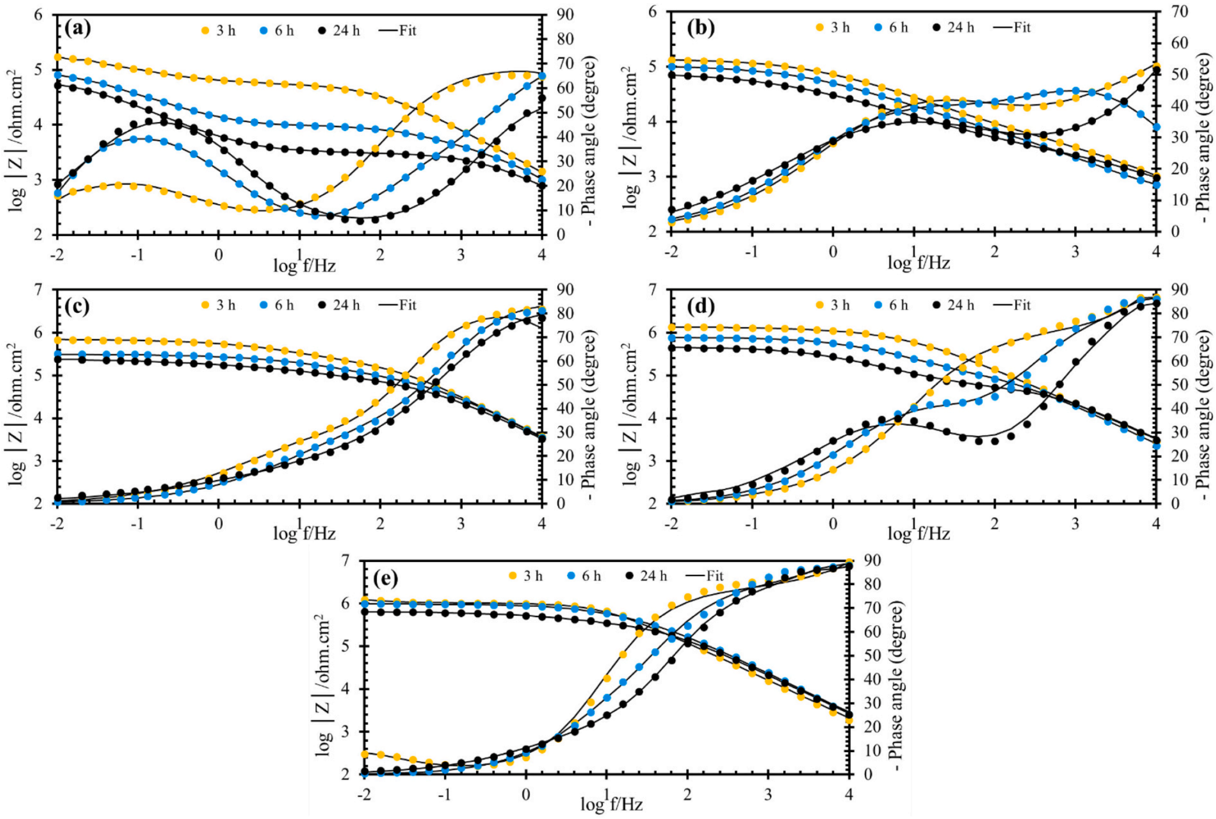

Fig. 8. Bode curves of the silane-based nanocomposites for Sil (a), Sil-C1 (b), Sil-C2 (c), Sil-C3 (d), and Sil-C4 (e) in different immersion times in the saline solution; The experimental and EEC fitting data are presented in forms of marker and solid line, respectively.

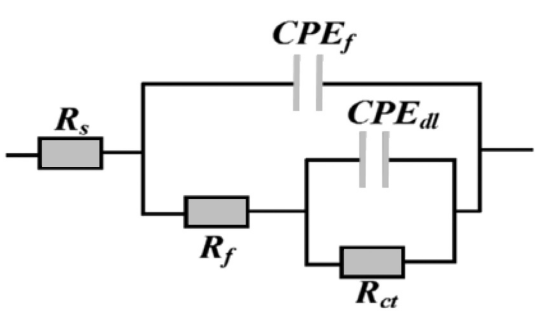

Fig. 9. The used EEC for fitting the EIS results in different immersion times.

be brought about that this proposed criterion was effective for the prediction model of different impedance Nyquist plots. The next step was to determine the number of epochs or in other words, the number of complete passes through the training dataset. The number of epochs is identified by utilizing the trial-and-error method [52]. The Root Mean Square (RMS) error is a function of the number of cycles as illustrated in Fig. 11. A range of 50 to 1000 epochs was tested and as shown in Fig. 11 the lowest RMSE value was obtained with 600 epochs.

After completing the network training process, the accuracy of the model can be evaluated by either a graphical representation of the data from the Nyquist plot and prediction results from the neural network outputs or calculation of the correlation coefficient. The experimental data from the Nyquist and Bode plots were compared with the simulated output from the ANN model in Figs. 12 and 13, illustrating a reliable agreement between simulated diagrams and experimental data.

The predictability of the ANN model or the correlation coefficient (R) takes values between −1 and 1 defined as follows:

$$R = \frac{\sum_{i=1}^{N}(y_i - \overline{y})(x_i - \overline{x})}{\sqrt{\sum_{i=1}^{N}(y_i - \overline{y})^2 \sum_{i=1}^{N}(x_i - \overline{x})}} \tag{6}$$

where x_i, y_i, $\overline{x}$, and $\overline{y}$ are the predicted output, actual data, mean of output, and an average of actual data, respectively. R^2 is the square of the correlation coefficient and its values range between 0 and 1. In particular, 1.0 shows a perfect correlation while 0.0 indicates no linear relationship between experimental and predicted data [53]. The linear regression line of predicted versus experimental component of the impedance is demonstrated in Fig. 14. As can be seen, no scattering could be distinguished in the entire data range and accordingly R^2 value was 0.9879. The reasonably high values reflected the reliable predictive power of the constructed model. The formula for the regression lines (best fitting line) was calculated and presented in Eq. (7).

$$y = 1.0317x + 3761.9 \tag{7}$$

Consequently, the constructed ANN model had a high level of adaptability and accuracy in predicting imaginary components of impedance, and accordingly, the Nyquist and Bode diagrams could be predicted over various concentrations of O-MWCNT in different immersion times.

3.2.6. *Polarization measurement*

The polarization examination was carried out for silane-based coated samples after 24 h immersion in 0.1 M NaCl solution depicted in Fig. 15. The positive impact of higher concentrations of O-MWCNTs could be clearly comprehended as the corrosion potential (E_{corr}) shifted to more noble values and the (i_{corr}) decreased significantly. To enumerate, i_{corr} for Sil, Sil-C1, Sil-C2, Sil-C3, and Sil-C4 samples equals to 5.40, 2.28,

Table 1
Electrochemical parameters obtained by fitting the experimental data with the appropriate EEC.

Sample	Immersion time (h)	R_{ct} (kΩ cm^2)[a]	CPE_{dl}		R_f (kΩ cm^2)[d]	CPE_f		$log \|Z\|_{10mHz}$
			Y_0 ($\mu\Omega^{-1}cm^{-2}$ s^n)[b]	n[c]		Y_0 ($\mu\Omega^{-1}cm^{-2}$ s^n)[e]	n[f]	
Sil	3	172.7	19.3	0.62	54.8	0.110	0.79	5.22
	6	96.3	39.4	0.70	9.1	0.250	0.75	4.90
	24	66.7	60.8	0.73	3.0	0.420	0.74	4.73
Sil-C1	3	89.5	1.51	0.61	55.4	0.120	0.74	5.12
	6	78.1	3.75	0.59	16.4	0.250	0.71	4.99
	24	75	7.56	0.57	4.5	0.430	0.70	4.85
Sil-C2	3	548.8	0.41	0.66	154.8	0.042	0.86	5.83
	6	257.1	0.49	0.65	54.1	0.066	0.84	5.50
	24	219.6	1.01	0.64	19.3	0.092	0.84	5.37
Sil-C3	3	380.3	0.75	0.55	984.4	0.017	0.88	6.09
	6	678.19	0.46	0.66	102.6	0.026	0.87	5.88
	24	417.6	0.81	0.65	52.2	0.038	0.85	5.64
Sil-C4	3	587.6	0.16	0.64	1020	0.016	0.88	6.12
	6	452.6	0.57	0.62	514.1	0.019	0.90	5.99
	24	359.5	0.79	0.61	286.5	0.022	0.89	5.81

[a] The standard deviation range for R_{ct} values was 3.6 %–12.5 %.
[b] The standard deviation range for Y_0 values was 3.0 %–10.7 %.
[c] The standard deviation range for n values was 1.9 %–9.0 %.
[d] The standard deviation range for R_f values was 4.8 %–9.7 %.
[e] The standard deviation range for Y_0 values was 5.3 %–9.6 %.
[f] The standard deviation range for n values was 2.6 %–8.5 %.

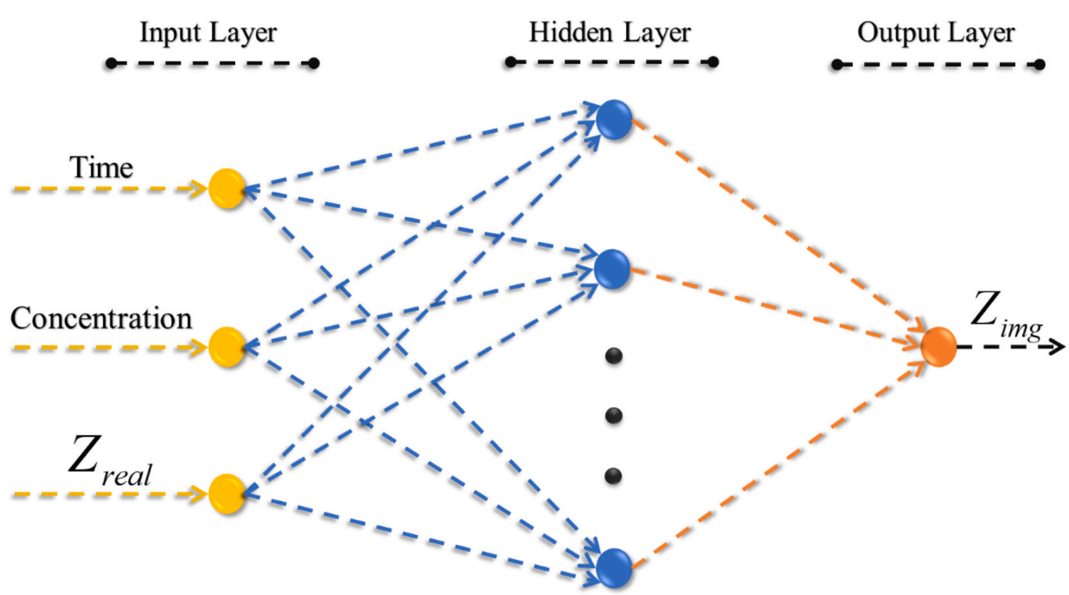

Fig. 10. The topological structure of the ANN model.

0.49, 0.23, and 0.04 μA/cm^2, respectively. The polarization outcome was in parallel with the EIS analysis, illustrating the enhancement of the barrier performance of the silane-based coating by increasing the number of O-MWCNTs in the silane network. It may arise from the thickening of the coatings along with the development of the cage-like structure of the silane network by increasing the intake of O-MWCNTs in silane formulation. Furthermore, the prolongation of diffusive pathways for aggressive elements could also play a crucial role in the barrier performance of the coating which is the highest for the Sil-C4 thanks to the highest amount of O-MWCNTs.

4. Conclusions

In this work, the pristine MWCNT was functionalized with the promising oxidation process certified with ZP, TGA, and XRD analyses. Different concentrations of obtained O-MWCNT were impregnated into the silane matrix to increase the barrier performance of the silane-based nanocomposite. The FE-SEM images illustrated that the thickness of the silane coating was heightened by increasing the content of O-MWCNT in the silane coating. The FT-IR and WCA measurements confirmed each other in making a more hydrophobic coating by increasing the incorporation of O-MWCNT. By increasing the content of O-MWCNT in the coating up to 0.9 % wt./wt., the barrier performance of the silane coating was enhanced confirmed by the EIS test. Moreover, the polarization analysis, in parallel with the EIS test, exhibited a significant depression of the corrosion current density by introduction of more O-MWCNTs into the silane coatings thanks to improvement in the barrier performance. Consequently, the diffusive pathways have been prolonged to initiate redox reactions on the substrate. Meanwhile, by taking advantage of ANN, the imaginary part of impedance in different immersion times related to the silane-based nanocomposites was predicted. In fact, the input variables were different concentrations of O-MWCNT, immersion time, and the real part of the impedance and consequently imaginary part of impedance was considered as the output

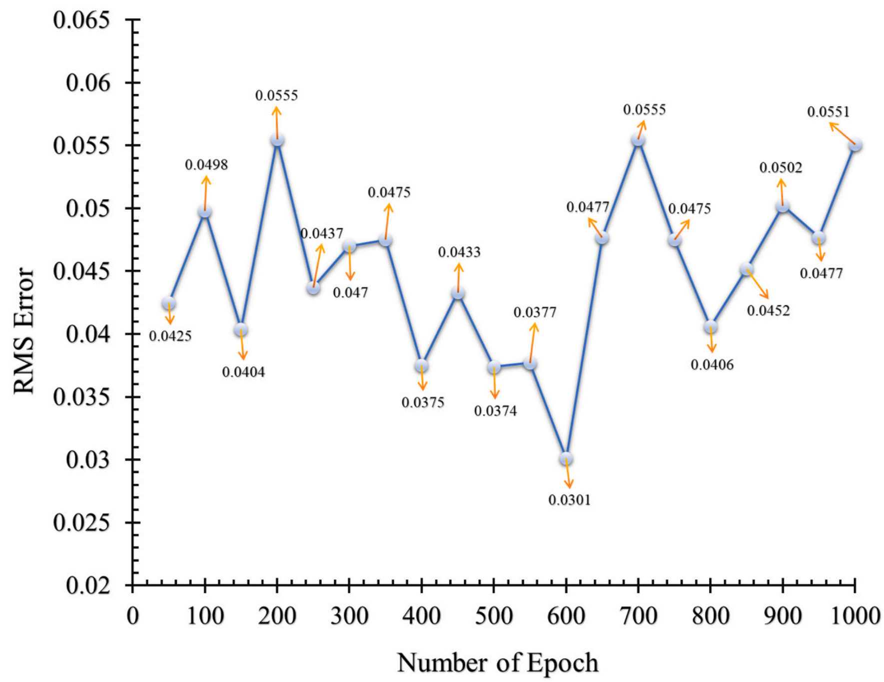

Fig. 11. Calculation of RMSE in the different number of epochs.

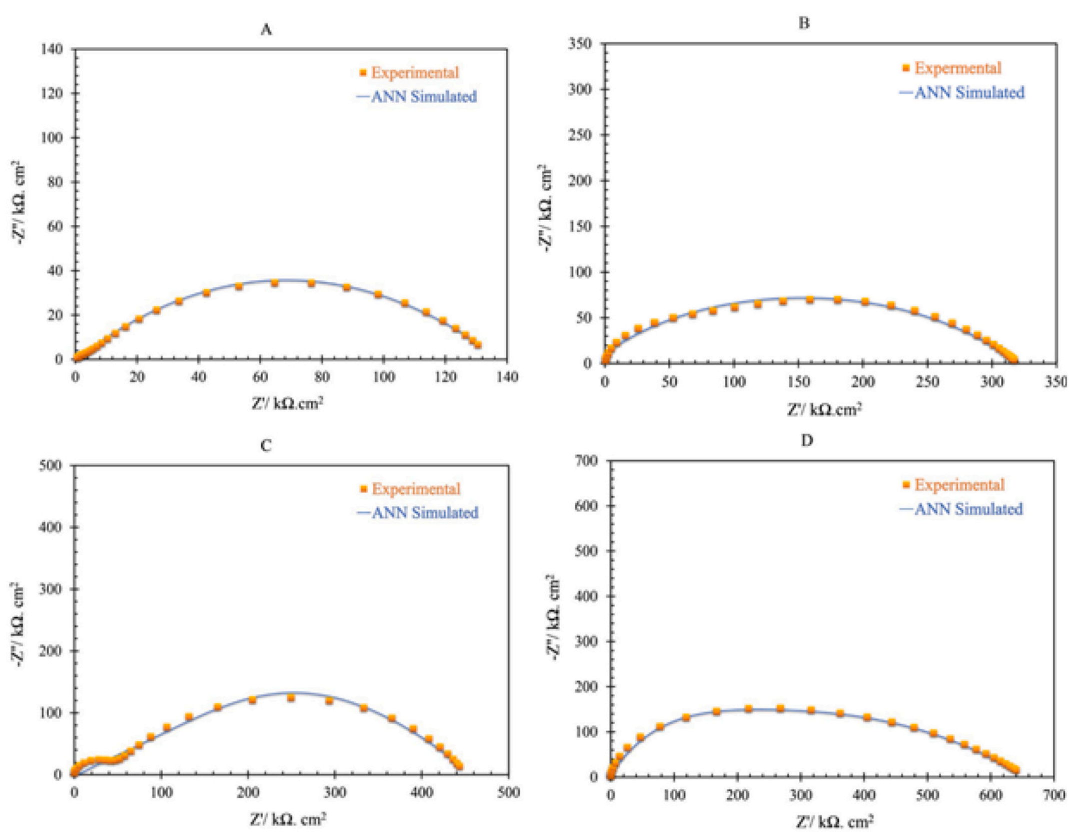

Fig. 12. Experimental versus simulated Nyquist diagrams for Sil-C1 after 3 h (A), Sil-C2 after 6 h (B), Sil-C3 after 24 h (C), and Sil-C4 after 24 h (D).

variable. Mathematically and graphically representation proved that the modeling was accurate enough to predict the imaginary component of impedance in different times of exposure and various usage of O-MWCNT in the silane solution.

Supplementary data to this article can be found online at https://doi.org/10.1016/j.porgcoat.2022.107296.

CRediT authorship contribution statement

Sajjad Akbarzadeh: Software, Formal analysis, Investigation,

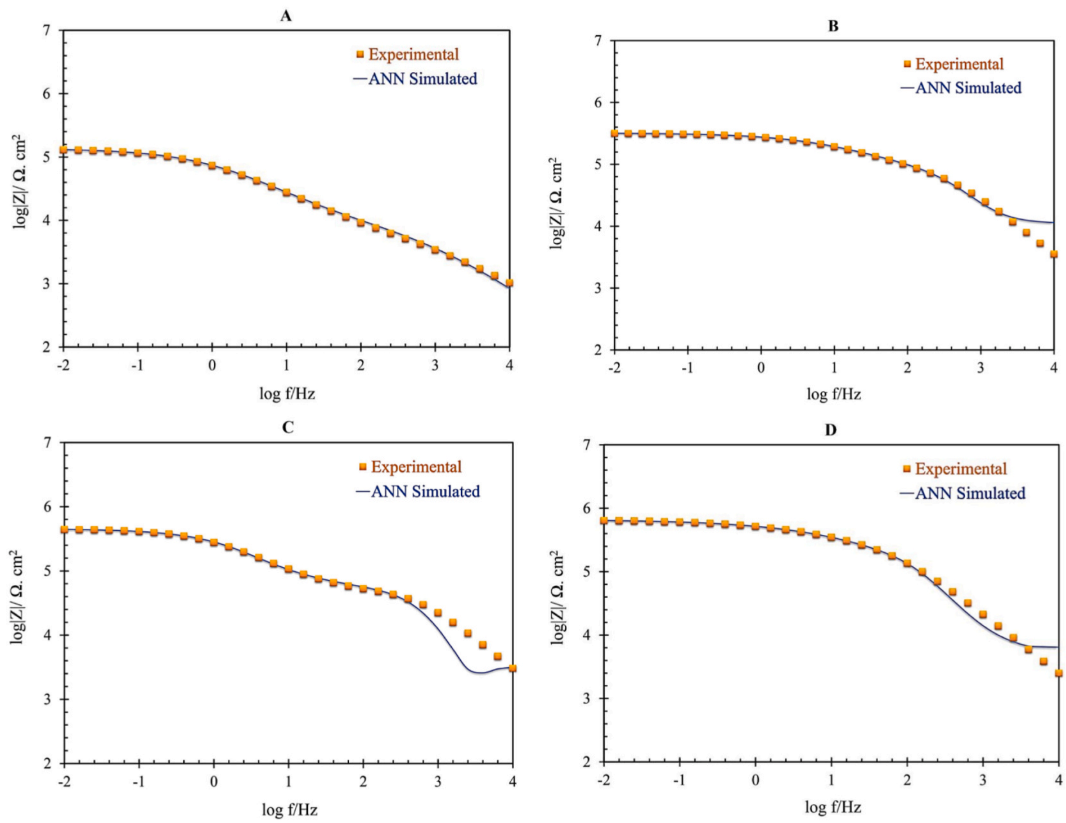

Fig. 13. The comparison of the simulated and experimental data in the Bode diagram related to Sil-C1 after 3 h (A), Sil-C2 after 6 h (B), Sil-C3 after 24 h (C), and Sil-C4 after 24 h (D).

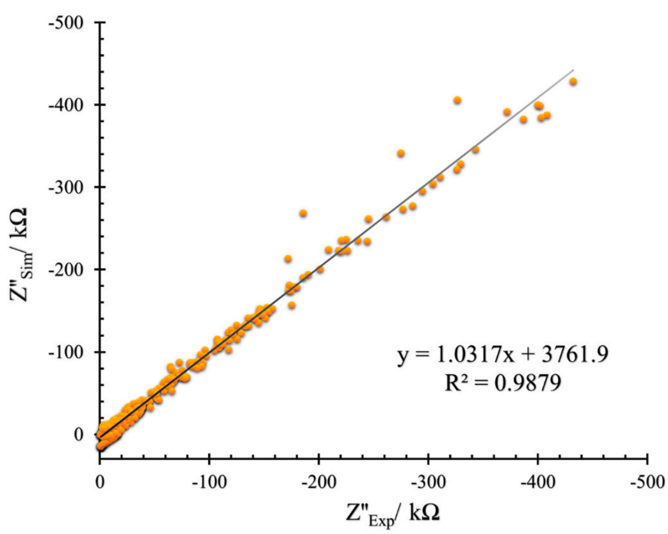

Fig. 14. The linear regression line between the predicted and experimental imaginary component of impedance.

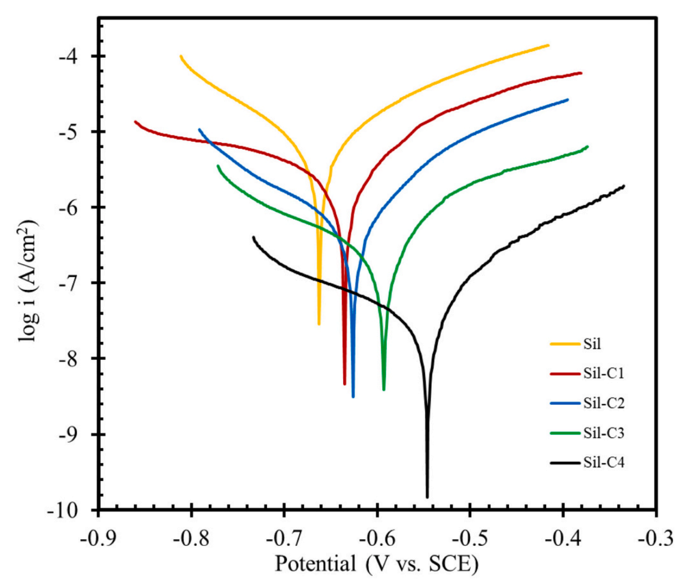

Fig. 15. Polarization curves of different silane-based coatings after 24 h immersion in 0.1 M NaCl solution.

Writing – original draft, Writing – review & editing. **Kazem Akbarzadeh:** Software, Formal analysis, Writing – original draft, Writing – review & editing. **Mohammad Ramezanzadeh:** Investigation. **Reza Naderi:** Conceptualization, Methodology, Resources, Writing – review & editing, Supervision. **Mohammad Mahdavian:** Conceptualization, Methodology, Resources, Writing – review & editing, Supervision. **Marie-Georges Olivier:** Conceptualization, Writing – review & editing.

Declaration of competing interest

The authors declare that they have no known competing financial interests or personal relationships that could have appeared to influence the work reported in this paper.

Data availability

Data will be made available on request.

References

[1] P.L. Bonora, F. Deflorian, L. Fedrizzi, Electrochemical impedance spectroscopy as a tool for investigating underpaint corrosion, Electrochim. Acta 41 (1996) 1073–1082.
[2] A. Amirudin, D. Thieny, Application of electrochemical impedance spectroscopy to study the degradation of polymer-coated metals, Prog. Org. Coat. 26 (1995) 1–28.
[3] A. Xu, F. Zhang, B. Luo, F. Jin, T. Zhang, Investigation the deterioration process of organic coating using changing rate of phase angle at high frequency united to neural network, Int. J. Electrochem. Sci. 8 (2013) 773–779.
[4] G. Kumar, R.G. Buchheit, Use of artificial neural network models to predict coated component life from short-term electrochemical impedance spectroscopy measurements, in: Corrosion, National Assoc. of Corrosion Engineers International, 2008, pp. 241–254.
[5] T. Breugelmans, E. Tourwé, J.B. Jorcin, A. Alvarez-Pampliega, B. Geboes, H. Terryn, A. Hubin, Odd random phase multisine EIS for organic coating analysis, Prog. Org. Coat. 69 (2010) 215–218.
[6] J.B. Jorcin, G. Scheltjens, Y. Van Ingelgem, E. Tourwé, G. Van Assche, I. De Graeve, B. Van Mele, H. Terryn, A. Hubin, Investigation of the self-healing properties of shape memory polyurethane coatings with the 'odd random phase multisine' electrochemical impedance spectroscopy, Electrochim. Acta 55 (2010) 6195–6203.
[7] S. Pletincx, J.M.C. Mol, H. Terryn, A. Hubin, T. Hauffman, An in situ spectro-electrochemical monitoring of aqueous effects on polymer/metal oxide interfaces, J. Electroanal. Chem. 848 (2019), 113311.
[8] M. Dabiri Havigh, B. Wouters, N. Hallemans, R. Claessens, J. Lataire, H. Terryn, A. Hubin, Operando odd random phase electrochemical impedance spectroscopy for in situ monitoring of the anodizing process, Electrochem. Commun. 137 (2022), 107268.
[9] A. Alvarez-Pampliega, T. Hauffman, M. Petrova, T. Breugelmans, T. Muselle, K. Van Den Bergh, J. De Strycker, H. Terryn, A. Hubin, Corrosion study on Al-rich metal-coated steel by odd random phase multisine electrochemical impedance spectroscopy, Electrochim. Acta 124 (2014) 165–175.
[10] T. Matias, F. Souza, R. Araújo, C.H. Antunes, Learning of a single-hidden layer feedforward neural network using an optimized extreme learning machine, Neurocomputing 129 (2014) 428–436.
[11] K.F. Khaled, N.A. Al-Mobarak, A predictive model for corrosion inhibition of mild steel by thiophene and its derivatives using artificial neural network, Int. J. Electrochem. Sci. 7 (2012) 1045–1059.
[12] M.Y. Rafiq, G. Bugmann, D.J. Easterbrook, Neural network design for engineering applications, Comput. Struct. 79 (2001) 1541–1552.
[13] D. Colorado-Garrido, D.M. Ortega-Toledo, J.A. Hernández, J.G. González-Rodríguez, J. Uruchurtu, Neural networks for nyquist plots prediction during corrosion inhibition of a pipeline steel, J. Solid State Electrochem. 13 (2009) 1715–1722.
[14] A. Bassam, D. Ortega-Toledo, J.A. Hernandez, J.G. Gonzalez-Rodriguez, J. Uruchurtu, Artificial neural network for the evaluation of CO 2 corrosion in a pipeline steel, J. Solid State Electrochem. 13 (2009) 773–780.
[15] M.R. Johan, S. Ibrahim, Neural networks for Nyquist plots prediction in a nanocomposite polymer electrolyte (PEO-LiPF6-EC-CNT), Ionics (Kiel) 17 (2011) 683–696.
[16] H. Méndez-Figueroa, D. Colorado-Garrido, M. Hernández-Pérez, R. Galván-Martínez, R. Orozco Cruz, Neural networks and correlation analysis to improve the corrosion prediction of SiO2-nanostructured patinated bronze in marine atmospheres, J. Electroanal. Chem. 917 (2022), 116396.
[17] C. Wang, W. Li, Y. Wang, X. Yang, S. Xu, Study of electrochemical corrosion on Q235A steel under stray current excitation using combined analysis by electrochemical impedance spectroscopy and artificial neural network, Constr. Build. Mater. 247 (2020), 118562.
[18] M. Ghobadi, D. Zaarei, R. Naderi, N. Asadi, S.R. Seyedi, M. Ravan Avard, Improvement the protection performance of lanolin based temporary coating using benzotriazole and cerium (III) nitrate: combined experimental and computational analysis, Prog. Org. Coat. 151 (2021), 106085.
[19] Z.S.H. Chan, H.W. Ngan, A.B. Rad, A.K. David, N. Kasabov, Short-term ANN load forecasting from limited data using generalization learning strategies, Neurocomputing 70 (2006) 409–419.
[20] M.W. Gardner, S.R. Dorling, Artificial neural networks (the multilayer perceptron) - a review of applications in the atmospheric sciences, Atmos. Environ. 32 (1998) 2627–2636.
[21] G. Singh, A. Professor, R.K. Panda, Daily sediment yield modeling with artificial neural network using 10-fold nross validation vethod: a small agricultural watershed, Kapgari, India, Int. J. Earth Sci. Eng. 4 (2011) 443–450.
[22] S. Akbarzadeh, M. Ramezanzadeh, B. Ramezanzadeh, M. Mahdavian, R. Naderi, Fabrication of highly effective polyaniline grafted carbon nanotubes to induce active protective functioning in a silane coating, Ind. Eng. Chem. Res. 58 (2019) 20309–20322.
[23] S.M. Orouji, R. Naderi, M. Mahdavian, Fabrication of protective silane coating on mild steel: the role of hydrogen peroxide in acid treatment solution, J. Ind. Eng. Chem. 64 (2018) 245–255.
[24] S.S. Rouzmeh, R. Naderi, M. Mahdavian, Steel surface treatment with three different acid solutions and its effect on the protective properties of the subsequent silane coating, Prog. Org. Coat. 112 (2017) 133–140.
[25] M.G. Olivier, M. Fedel, V. Sciamanna, C. Vandermiers, C. Motte, M. Poelman, F. Deflorian, Study of the effect of nanoclay incorporation on the rheological properties and corrosion protection by a silane layer, in: Prog. Org. Coatings, Elsevier, 2011, pp. 15–20.
[26] S. Akbarzadeh, R. Naderi, M. Mahdavian, Fabrication of a highly protective silane composite coating with limited water uptake utilizing functionalized carbon nano-tubes, Compos. Part B Eng. 175 (2019), 107109.
[27] H. Hu, A. Yu, E. Kim, B. Zhao, M.E. Itkis, E. Bekyarova, R.C. Haddon, Influence of the zeta potential on the dispersability and purification of single-walled carbon nanotubes, J. Phys. Chem. B 109 (2005) 11520–11524.
[28] Y.J. Kim, T.S. Shin, H. Do Choi, J.H. Kwon, Y.C. Chung, H.G. Yoon, Electrical conductivity of chemically modified multiwalled carbon nanotube/epoxy composites, Carbon N. Y. 43 (2005) 23–30.
[29] S. Gómez, N.M. Rendtorff, E.F. Aglietti, Y. Sakka, G. Suarez, Intensity of sulfonitric treatment on multiwall carbon nanotubes, Chem. Phys. Lett. 689 (2017) 135–141.
[30] D. Chudoba, K. Łudzik, M. Jażdżewska, S. Wołoszczuk, Kinetic and equilibrium studies of doxorubicin adsorption onto carbon nanotubes, Int. J. Mol. Sci. 21 (2020) 8230.
[31] V. Datsyuk, M. Kalyva, K. Papagelis, J. Parthenios, D. Tasis, A. Siokou, I. Kallitsis, C. Galiotis, Chemical oxidation of multiwalled carbon nanotubes, Carbon N. Y. 46 (2008) 833–840.
[32] S.K. Yadav, S.S. Mahapatra, M.K. Yadav, P.K. Dutta, Mechanically robust biocomposite films of chitosan grafted carbon nanotubes via the [2 + 1] cycloaddition of nitrenes, RSC Adv. 3 (2013) 23631–23637.
[33] A. Madhankumar, N. Rajendran, A promising copolymer of p-phenylendiamine and o-aminophenol: chemical and electrochemical synthesis, characterization and its corrosion protection aspect on mild steel, Synth. Met. 162 (2012) 176–185.
[34] T. Jeevananda, T.S. Siddaramaiah, J.H. Lee, O.M. Lee, R. Samir, Somashekar, polyaniline-multiwalled carbon nanotube composites: characterization by WAXS and TGA, J. Appl. Polym. Sci. 109 (2008) 200–210.
[35] Y. Peng, H. Liu, Effects of oxidation by hydrogen peroxide on the structures of multiwalled carbon nanotubes, Ind. Eng. Chem. Res. 45 (2006) 6483–6488.
[36] J. Yan, L.F. Yi, W.R. Zhong, Catalytic growth of carbon-nianotubes with large inner diameters, J. Serbian Chem. Soc. 70 (2005) 277–282.
[37] S.L. Zhang, X. Hu, H. Li, Z. Shi, K.T. Yue, J. Zi, Z. Gu, X. Wu, Z. Lian, Y. Zhan, F. Huang, L. Zhou, Y. Zhang, S. Iijima, Abnormal anti-stokes Raman scattering of carbon nanotubes, Phys. Rev. B - Condens. Matter Mater. Phys. 66 (2002) 354131–354135.
[38] N. Parhizkar, B. Ramezanzadeh, T. Shahrabi, Enhancement of the corrosion protection properties of a hybrid sol-gel based silane film through impregnation of functionalized graphene oxide nanosheets, J. Electrochem. Soc. 164 (2017) C1044–C1058.
[39] M. Fedel, E. Callone, S. Diré, F. Deflorian, M.G. Olivier, M. Poelman, Effect of Na-Montmorillonite sonication on the protective properties of hybrid silica coatings, Electrochim. Acta 124 (2014) 90–99.
[40] F. Deflorian, S. Rossi, L. Fedrizzi, M. Fedel, Integrated electrochemical approach for the investigation of silane pre-treatments for painting copper, Prog. Org. Coat. 63 (2008) 338–344.
[41] S. Akbarzadeh, L. Sopchenski Santos, V. Vitry, Y. Paint, M.G. Olivier, Improvement of the corrosion performance of AA2024 alloy by a duplex PEO/clay modified sol-gel nanocomposite coating, Surf. Coat.Technol. 434 (2022), 128168.
[42] B. Orel, R. Ješe, A. Vilčnik, U.L. Štangar, Hydrolysis and solvolysis of methyltriethoxysilane catalyzed with HCl or trifluoroacetic acid: IR spectroscopic and surface energy studies, J. Sol-Gel Sci. Technol. 343 (34) (2005 2005) 251–265.
[43] V. Tagliazucca, E. Callone, S. Dirè, Influence of synthesis conditions on the cross-link architecture of silsesquioxanes prepared by in situ water production route, J. Sol-Gel Sci. Technol. 60 (2011) 236–245.
[44] M.F. Montemor, M.G.S. Ferreira, Cerium salt activated nanoparticles as fillers for silane films: evaluation of the corrosion inhibition performance on galvanised steel substrates, Electrochim. Acta 52 (2007) 6976–6987.
[45] P. Molaeipour, S.R. Allahkaram, S. Akbarzadeh, Corrosion inhibition of Ti6Al4V alloy by a protective plasma electrolytic oxidation coating modified with boron carbide nanoparticles, Surf. Coat.Technol. 430 (2022), 127987.
[46] P. Molaeipour, M. Ramezanzadeh, B. Ramezanzadeh, Stachys byzantina extract: a green biocompatible molecules source for graphene skeletons generation on the carbon steel for superior corrosion mitigation, Bioelectrochemistry 143 (2022), 107970.
[47] T. Rolich, I. Rezić, L. Ćurković, Estimation of steel guitar strings corrosion by artificial neural network, Corros. Sci. 52 (2010) 996–1002.
[48] T. Parthiban, R. Ravi, G.T. Parthiban, S. Srinivasan, K.R. Ramakrishnan, M. Raghavan, Neural network analysis for corrosion of steel in concrete, Corros. Sci. 47 (2005) 1625–1642.
[49] V. Díaz, C. López, Discovering key meteorological variables in atmospheric corrosion through an artificial neural network model, Corros. Sci. 49 (2007) 949–962.
[50] K.G. Sheela, S.N. Deepa, Review on methods to fix number of hidden neurons in neural networks, Math. Probl. Eng. 2013 (2013).
[51] K. Jinchuan, L. Xinzhe, Empirical analysis of optimal hidden neurons in neural network modeling for stock prediction, in: Proc. - 2008 Pacific-Asia Work. Comput.

Intell. Ind. Appl. PACIIA 2008, 2008, pp. 828–832, https://doi.org/10.1109/PACIIA.2008.363.

[52] D. Ok, Y. Pu, A. Incecik, Artificial neural networks and their application to assessment of ultimate strength of plates with pitting corrosion, Ocean Eng. 34 (2007) 2222–2230.

[53] K. Akbarzade, I. Danaee, Nyquist plots prediction using neural networks in corrosion inhibition of steel by Schiff base, Iran. J. Chem. Chem. Eng. 37 (2018) 135–143.